Chemical Engineering Journal 455 (2023) 140815

Contents lists available at ScienceDirect

Chemical Engineering Journal

journal homepage: www.elsevier.com/locate/cej

Ultrafine powder coating: Smooth surface, dense structure and enhanced corrosion resistance

Jinbao Huang [a,f], Marshall Yang [a], Libin Wan [a], Keyong Tang [b], Hui Zhang [a,*], Jian Chen [c], James J Noël [c], Ivan Barker [d], Haiping Zhang [e], Jesse Zhu [a]

[a] Department of Chemical and Biochemical Engineering, Western University, London, Ontario N6A 5B9, Canada
[b] School of Materials Science and Engineering, Zhengzhou University, Zhengzhou 450001, China
[c] Department of Chemistry, The University of Western Ontario, London N6A 5B7, Canada
[d] Surface Science Western, The University of Western Ontario, London N6G 0J3, Canada
[e] School of Chemical Engineering and Technology, Tianjin University, Tianjin 300350, China
[f] Zhengzhou Research Institute, Harbin Institute of Technology, Zhengzhou, Henan 450000, China

ARTICLE INFO

Keywords:
Ultrafine powder coatings
Dense structure
Corrosion protection
Electrochemical impedance
Confocal laser scanning microscopy
Leveling

ABSTRACT

In recent years, powder coatings are capturing more of the liquid coatings market due to their economical, ecological, environmental, and energy-saving benefits, yet their low surface qualities still hinder their wider application. In this study, ultrafine powder coatings (~22 μm in size) were fabricated and compared with coarse powder coatings (~35 μm in size) in terms of particles deposition during spray, leveling of coating powder during curing, and surface qualities, inner structures, and anti-corrosive properties of the obtained coating films. The results show that the ultrafine particles pack more loosely and uniformly during spraying with smaller average air pockets and level and degas faster during curing than their coarse counterparts. These characters lead the ultrafine powder to demonstrate lower surface roughness, higher gloss, fewer inner voids, and higher corrosion resistance. The significant increase in corrosion performance is exhibited through high barrier properties and narrow salt spray creepage. This study contributes not only to the in-depth understanding of how particle size affects coating film structure and properties, such as gloss, surface roughness and corrosion protection, but also to the promotion of powder coating technology in broader fields such as electronics and automotive industries.

1. Introduction

Powder coatings contain no volatile solvents and have ecological, excellence of finish, economic, and energy-saving advantages when compared with liquid coatings [1–4]. For example, the over-sprayed powder can be reclaimed and reused [5]. The elimination of costly solvents generates fewer voids and pores inside the coatings, creating a denser coating film [6]. When compared with water-based liquid coatings bearing a large number of hydrophilic groups to realize dispersion in water [7], powder coatings require no such complex chemical modification, and have lower water permeability than the water-based ones [8]. The dense structure and water-resistant nature enables powder coatings to demonstrate high barrier effect against corrosive environment [6,9]. In addition, a thick powder coating film can be efficiently applied through a single spray, and a coating film can be obtained after a short curing of only 15 min, ultimately increasing production efficiency [5]. Due to these advantages, powder coatings have gained popularity as a coating for architectural structures, furniture, home appliances, and outdoor facilities [1,5,10].

Specific challenges exist that hinder the broader application of powder coatings. One of the challenges is the relatively lower surface smoothness and excessive film thickness [5], which can prevent powder coatings from being applied to high-end products such as car bodies, personal electronics and other articles with high aesthetic requirements. Decreasing the average particle size or eliminating large particles in the regular coarse powder coatings (medium particles size, D50 is above 30 μm) have been shown to provide a smooth surface [5,11]. However, decreased particle size can also cause problems in fluidization, which is a basic operation in powder coating application. Fine (D50 is between 25 and 30 μm) and ultrafine powder coatings (D50 is smaller than 25 μm) [11] have a higher content of small particles, which have strong inter-particle forces resulting from van der Waal's forces [12,13]. This

* Corresponding author.
E-mail address: hzhang1@uwo.ca (H. Zhang).

https://doi.org/10.1016/j.cej.2022.140815
Received 13 July 2022; Received in revised form 23 October 2022; Accepted 4 December 2022
Available online 6 December 2022

results in these smaller particles tending to form agglomerates and clumps in fluidization [14]. To overcome this issue, flow additives can be incorporated to enhance the fluidization of ultrafine powders [13–20]. Zhu and Zhang [11,14] have successfully applied powders with an average size of about 20 μm by adding a small dose of nanoparticles as flow additives. These additives are characterized by low-bulk-density, amorphous nano metal oxides in branched, chainlike, three-dimensional morphology. Once incorporated into an ultrafine coating powder (the host particles) by dry blending, the sub-micrometer size agglomerates of the additive adhere to the host particles and effectively increase the inter-particle distance, reduce the inter-particle forces and subsequently, enhance the flowability of the ultrafine powder. With the use of ultrafine powder, high aesthetic surface quality and thin film finishing were achieved [11]. Subsequently, more investigations were carried out on the manufacturing [21,22], fluidization [17,23–29], electrostatic spraying and recycling of ultrafine powder [30–34]. For example, the studies by Meng et al. and Li et al. on the charging and deposition of ultrafine particles revealed that finer particles have higher powder packing uniformity [30,35]. These fundamental studies boosted the development of functional finishes, such as superhydrophobic coatings [36,37], antimicrobial coatings [17,24,38] and their applications for general purposes [38–41], biomedical [42–44], and pharmaceutical uses [45].

However, the formation mechanism of smoother surface, the effects of the ultrafine powders on the coating film structure and on coating properties such as corrosion performance are poorly understood. In particular, protection against corrosion is one of the main roles of a coating and is closely related to the film structure [46,47]. Coating films with more voids and channels usually lead to a lower barrier effect and protection against corrosion than the ones with a denser structure [9,48].

This study includes preparation of both coarse and ultrafine powder coatings to compare their film surface qualities, inner structures, leveling of powder during curing and corrosion protection abilities. Polyester powder coatings can be used for both indoor and outdoor applications and are occupying the majority of general use powder coating market. Therefore, a general use polyester powder coating was selected as the model. In addition, the mechanisms behind the improved performances were a focus. The results could benefit coating manufacturers and applicators to produce thin film finishing with higher surface quality and enhanced corrosion performance and expand the applications of powder coatings to the high-end industrial sectors such as electronics and automotive industries.

2. Experimental

2.1. Materials

Polyester (PE) powder coating was procured from TCI Powder Coatings Co., Ltd., (USA). This coating includes carboxyl-terminated polyester as base resin, triglycidyl isocyanuate as curing agent, barium sulphate as filler, carbon black as pigment, benzoin as degassing agent, and other additives such as leveling agent. Powder flow additive Aerosil 200 (fumed silica) was purchased from Evonik Industries AG (Germany). Standard Q-panel steel substrates (S-36-I phosphated steel substrate) were purchased from Q-Lab Corporation (USA).

2.2. Preparation of ultrafine coating powders and coated panels

As shown in Fig. 1, 100 g polyester coating powder with a D50 of 35.0 μm was mixed with 0.6 g of Aerosil 200 (fumed silica) [17]. The mixture was further pulverized into ultrafine particles (D50 of about 22.0 μm) with a laboratory superfine grinder (FDV grinder, Youqi, Co., ltd, China). The detailed particle size distribution and SEM images were shown Fig. S1. The obtained powder was sprayed onto a steel substrate with an electrostatic spraying gun (ITW Gema, Switzerland) in a powder coating spraying booth (N902, Nordson Corporation, USA) at −30 kV and at 20 cm away from the substrate. During spraying, the particles became charged and flew towards the steel substrate with airflow and deposited on the substrate surface. All coated panels were cured at 200 °C for 15 min. During curing, the particles were melted and leveled under heat, which caused the resin and hardening agent to become

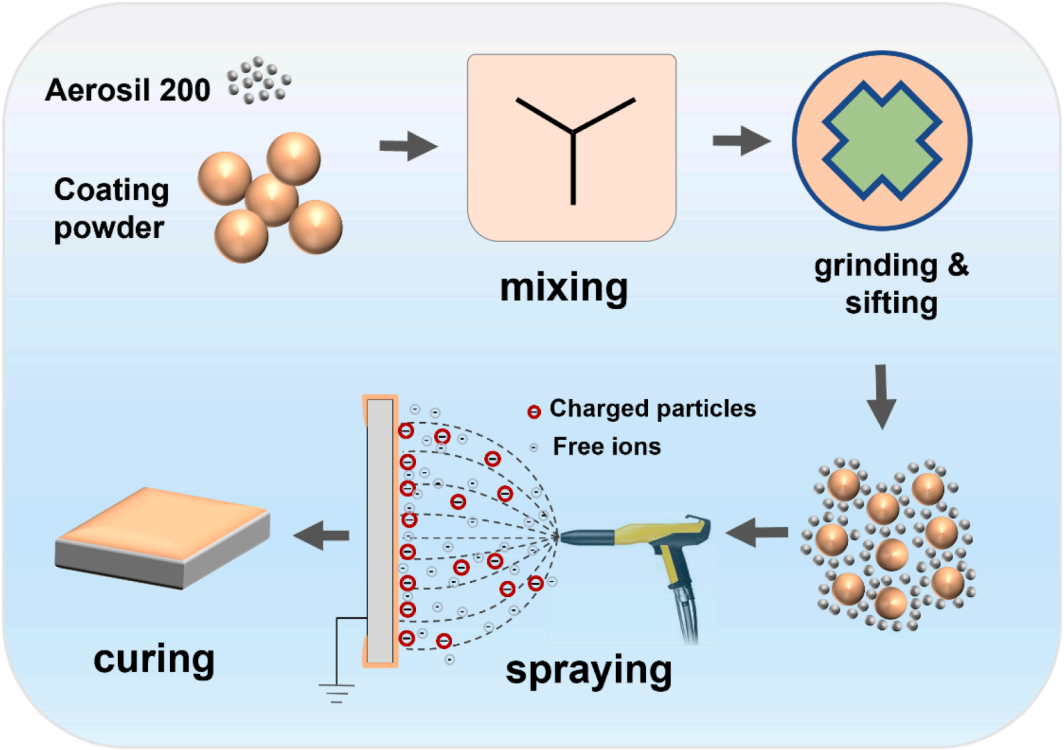

Fig. 1. Fabrication process of ultrafine powder coatings.

cross-linked. In comparison, regular coarse powder coatings were sprayed at −50 kV, a commonly used voltage for coarse coatings. The obtained coatings had film thickness of about 40 μm.

2.3. Surface and cross-sectional morphologies

The surface morphology was characterized using multiple techniques including optical microscopy (VHX-950F, Keyence, Japan) and confocal laser scanning microscopy (CLSM 900 for Materials, Carl Zeiss Microscopy, Germany). The acquired confocal data were processed through ConfoMap version 7.4.8341, which provided 3D images on microstructures and quantitative analysis on surface waviness and roughness. The specular gloss of the obtained coating films was measured with a Rhopoint IQ 20/60 gloss meter (Rhopoint Instruments Ltd., UK) as per ASTM D523-14.

To characterize the cross-sectional structures of the powder coatings on the substrate, the coated panels were mounted in epoxy, sectioned, and polished to a mirror like finish using standard techniques. The polished cross-sections were analyzed by scanning electron microscopy (SEM, SU3900, Hitachi, Japan) with an accelerating voltage of 10 kV. The cross-sectional SEM images were processed with the software Image J to obtain the area ratio of voids inside the coating films. The processing was implemented in a three steps procedure: converting the images into greyscales, adjusting threshold to obtain areas representing voids, and calculating the area ratios. Calculations on at least three images gave an average value.

2.4. Powder deposition during spray and leveling during curing

As there is no in line method to monitor real-time leveling of powder during curing, an offline method was proposed. It was implemented by preparing identical powder-deposited panels, having these panels cured for 0, 10, 15, 30, 60, 180 and 900 s, respectively, and characterizing the surface morphologies and inner structures of the obtained coating films.

The deposition behaviors of ultrafine and coarse particles on metallic substrate before curing were characterized on the samples cured for 0 s using X-ray Micro Computed Tomography (Zeiss Xradia 410 Versa Micro-CT, Germany) at 80 kV and 10 W. The obtained images were processed with ORSI's Dragonfly and the software Image J to produce 3 dimensional images of the powder deposition layer and to assess the air content inside the deposited powder.

The changes in surface morphologies and gloss as the powder leveled during curing were characterized using optical microscopy, CLSM and a gloss meter on the samples cured for 10, 15, 30, 60, 180 and 900 s, respectively. The changes in inner structures during curing were characterized using SEM. To avoid melting of the insufficiently cured coatings, the samples were sputtered with gold before mounting.

To investigate the formation of local hills and valleys on the film surfaces, an integrated study using optical microscopy, CLSM and Micro CT was undertaken. Artificial fiducial marks were made for positioning and alignment between these techniques.

2.5. Salt spray and corrosion tests

Two 0.5 mm intersecting scribes were made on the coating panels before neutral salt spray tests were conducted, as per ASTM B117-16 in a salt spray chamber (MX-9204, Associated Environmental Systems, USA). The performances of the coatings after salt spray tests were evaluated after 500 h as per ISO 4628–8. The corrosion progression was measured normal to scribe direction, and at least 12 measurements yielded an average value of corrosion width. The average creepage was calculated by subtracting the average value of corrosion width by the scribe width (0.5 mm) and dividing by two.

To investigate the corrosion behaviors of the ultrafine and coarse powder coatings under immersion, EIS measurements were carried out with an integrated potentiostat, (Solartron Analytical Modulab XM CHAS 08, AMETEK Scientific Instruments, Oak Ridge, TN, USA). The electrochemical experiments were performed in 3.5 wt% NaCl solution in a three-electrode system. A saturated calomel electrode (SCE) worked as the reference electrode, a platinum foil as the counter electrode and the coated panel as the working electrode. The exposed area of the coated panel was 20.25 cm^2. EIS measurements were conducted from 10^5 Hz to 0.01 Hz. The sinusoidal voltage signal amplitude was set as 70 mV due to relatively high resistance (higher than 10MΩ cm^2) at low frequency range [49].

3. Results and discussion

3.1. Surface qualities

A coating film's decoration, which is related to its surface qualities such as gloss and roughness, is one of the most important features. The 60-degree gloss and surface roughness were measured, and topographical microstructure was characterized to evaluate these surface qualities. Optical microscopy images presented in Fig. 2a and b, show that the coarse powder coating film has larger topography, including many larger hills and valleys that are ~1000 μm wide and some smaller bits (local seeds like protuberances) and pits (local craters) of ~50 μm on the surface, while the ultrafine coating films possess much smaller hills and valleys and fewer bits and pits. As a result, the ultrafine coating films show a higher gloss than the coarse one. The gloss increases from 86.9 to 89.3. The gloss increased from 86.9 to 89.3. This increase is significant because enhancing the gloss of a high gloss coatings is not easy due to its high leveling ability. A small increase in gloss usually requires apparent increase in leveling ability.

As opposed to the 60-degree gloss and optical microscopy methods, CLSM is an efficient optical device for characterizing surface morphology and is often applied in material and coatings studies [37,50]. It provides quantitative information such as surface waviness and roughness. As shown in Fig. 2c and g, for a relatively large area (9.6 mm × 9.6 mm) including hills and valleys, bits and pits, the coarse coating film shows more and higher hills than the ultrafine film. The arithmetic average surface roughness (Sa) of the coarse coating is 0.79 μm, while Sa for the ultrafine one is 0.57 μm. The maximum height (Sz, the sum of the largest peak height and the largest valley), is 5.90 μm and 4.80 μm for the coarse and ultrafine, respectively. When a surface profile (the yellow horizontal line) was extracted from the 3D surface, it was further separated into long-range waviness and short-range roughness (Fig. 2d–f, h and i), corresponding to ~1000 μm wide large hills and valleys, and the ~50 μm wide smaller bits and pits. It is found that the lower particle size led to decreased waviness and roughness, indicating that decreasing the particle size to ~20 μm is an effective method to improve surface qualities.

3.2. Inner structures of the coating films

The ability of a coating film to protect the underlying substrate is another very important attribute, and its protection abilities are closely related to the coating's inner structures. Fig. 4 presents a series of cross-sectional SEM images showing the inner structures of the PE coating films. Generally, the coating films display voids of ~1 μm inside the film. However, the coating film prepared from ultrafine powders (Fig. 3b) demonstrates smaller and fewer voids than those from coarse powder (Fig. 3a), as indicated by the red arrows. This dense structure could bring better barrier properties for these films, which will be discussed in the anti-corrosion section below.

3.3. Deposition of powder during spray and leveling during curing

Ultrafine powder offers smoother surfaces and denser inner structure than the coarse powder, which is possibly due to how the powders were deposited during spray and leveled during curing. Fig. 4a and b show the

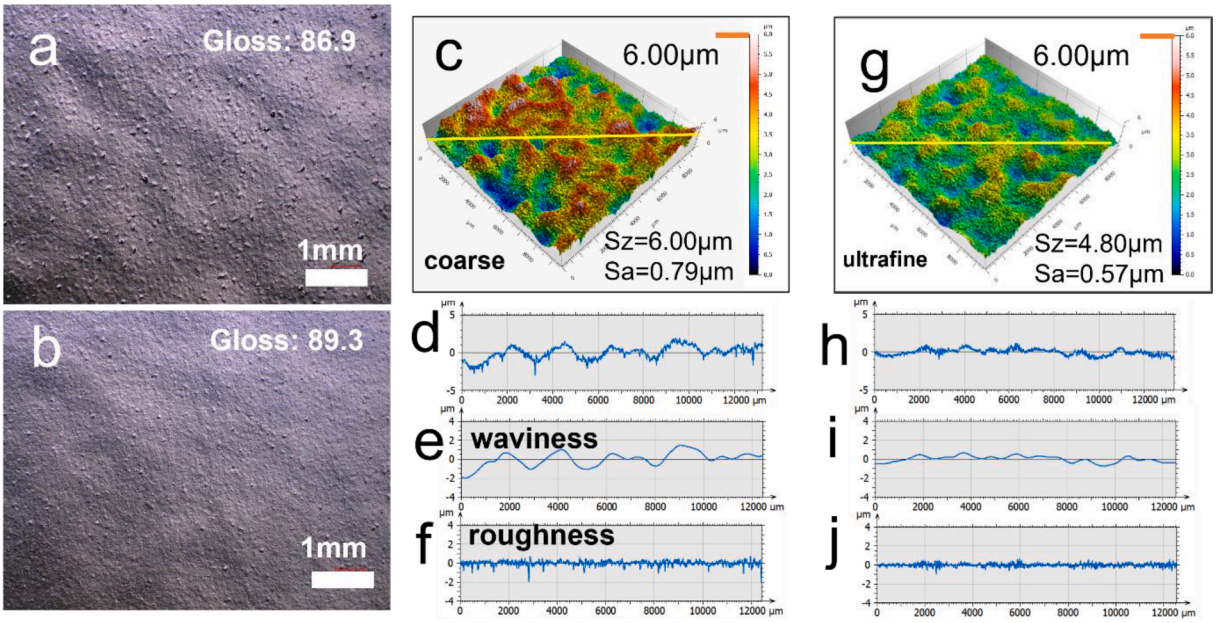

Fig. 2. Optical images of (a) coarse and (b) ultrafine powder coating films; 3D CLSM images of coating films prepared with (c) coarse and (g) ultrafine powders; (d) profile along the yellow line in (c) and the corresponding (e) waviness and (f) roughness; (h) profile of the yellow line in (g) and the corresponding (i) waviness and (j) roughness.

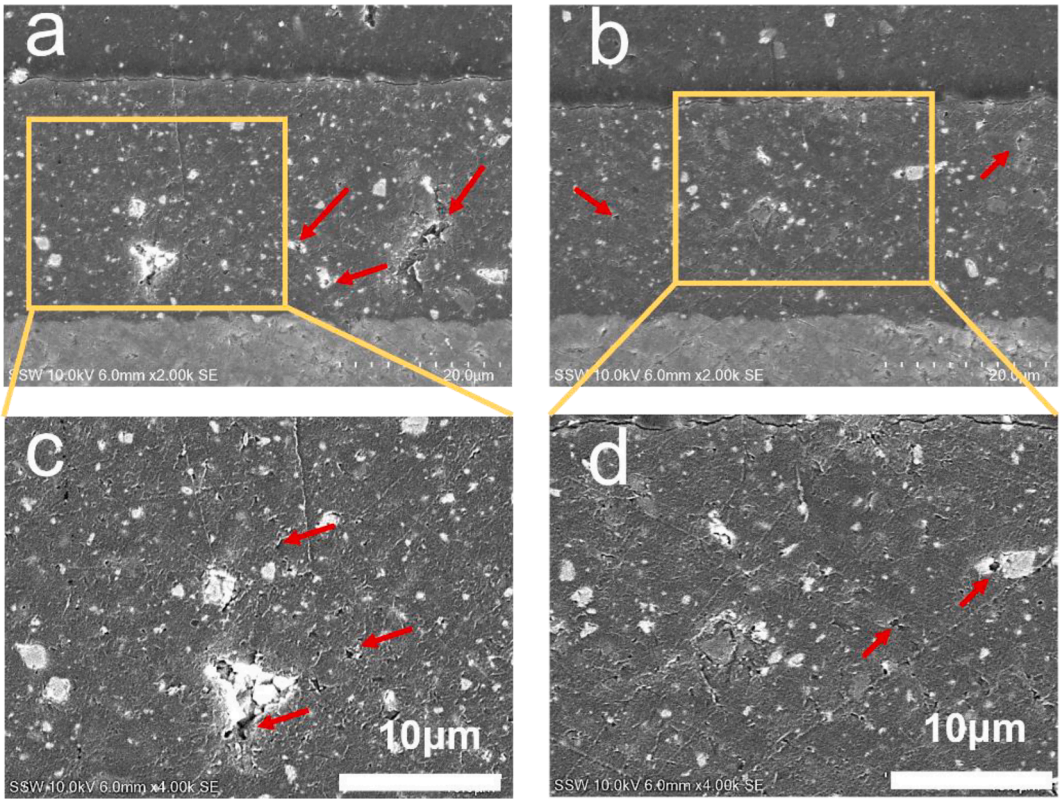

Fig. 3. SEM images of coarse (a) and ultrafine (b) powder coating films. (c) magnification of (a), (d) magnification of (b). Red arrows point to voids.

3D Micro CT block model images of the ultrafine and coarse powder deposited on the substrate, which are generally loose and in a uniform packing pattern. At the top of the deposition layers, individual particles and the spaces around them formed local microscale roughness, and their aggregates of hundreds of micrometers could be observed as hills and valleys. The ultrafine particles packed more evenly with smaller hills and shallower valleys than the coarse ones. These behaviors of ultrafine powder agree well with previous report and simulation on the deposition behavior of ultrafine powder coatings [30,35,51]. Fig. 4c and d show that the air content for the ultrafine powder in the deposited layer is higher (49.6 %) than that of the coarse powder (36.6 %), and the overall packing thickness is also higher for the ultrafine powder (93 μm) than the coarse powder (72 μm) for obtaining the same film thickness. However, the average diameter of the air pockets among the ultrafine

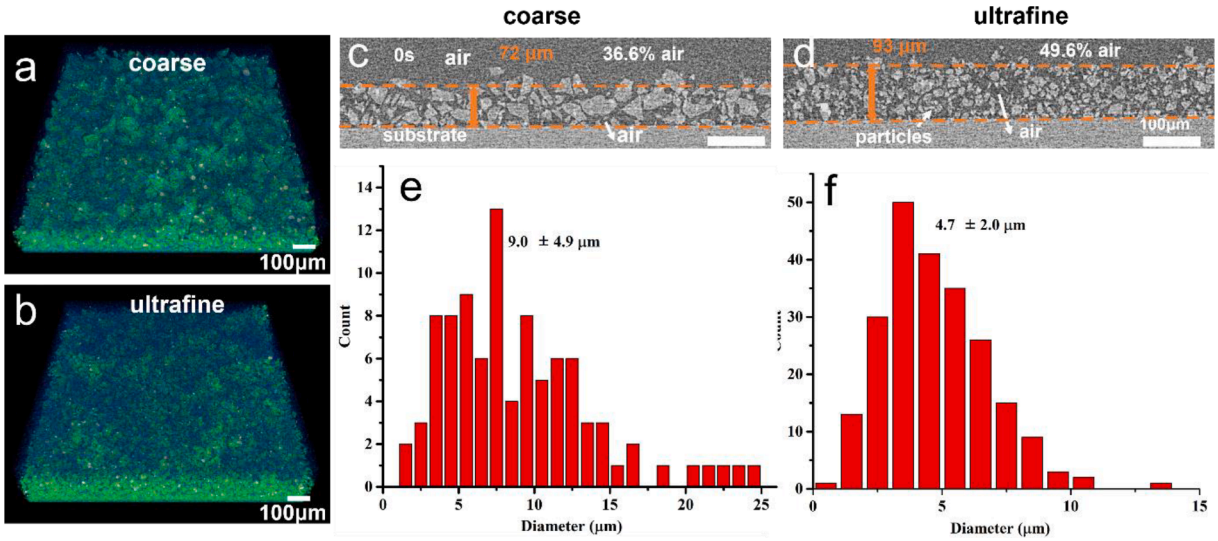

Fig. 4. Micro CT 3D block model images of deposited layer prepared form high gloss PE coarse (a) and ultrafine (b) coating powder. Micro CT 2D cross sectional images of high gloss (c) coarse and (d) ultrafine powder deposits. Air pocket size distribution measured with Image J for (e) coarse and (f) ultrafine powder deposits from (c) and (d), respectively.

particles is much smaller (4.7 μm) than that for coarse particles (9.0 μm) as shown in Fig. 4e and f. In addition, the largest air pocket among ultrafine particles is about 13 μm, while for the coarse particles, it is about 25 μm.

The differences in deposition are attributed to the charging behaviors of coating particles. Coating particles picked up negative ions when passing through the charged zone [52], repelled each other under electrostatic forces in flying [53], and adhered to the substrate with image charges [54,55]. However, smaller particles have a higher charge to mass ratio and a higher charging efficiency [52,56,57], and are determined more by electrostatic forces instead of the gravity during spraying. As a result, the coarse particles with a size ranging from 2 μm to over 100 μm (Fig. S1) are deposited on the substrate closely with each other, but cause porosity in between the particles, resulting in a high packing density and a large average size of air pockets. The smaller particles with a size ranging from 1 μm to 60 μm (Fig. S1) tend to repel each other due to strong electrostatic forces, causing looser and more uniform deposition structures, but with a smaller average air pocket.

The air sparces in between the particles dissipate during curing when the individual particles melted, and then merged and levelled to form a continuous coating film [1]. Benzoin, as the degassing agent, can facilitate the removal of gas bubbles by accelerating the rate of bubble

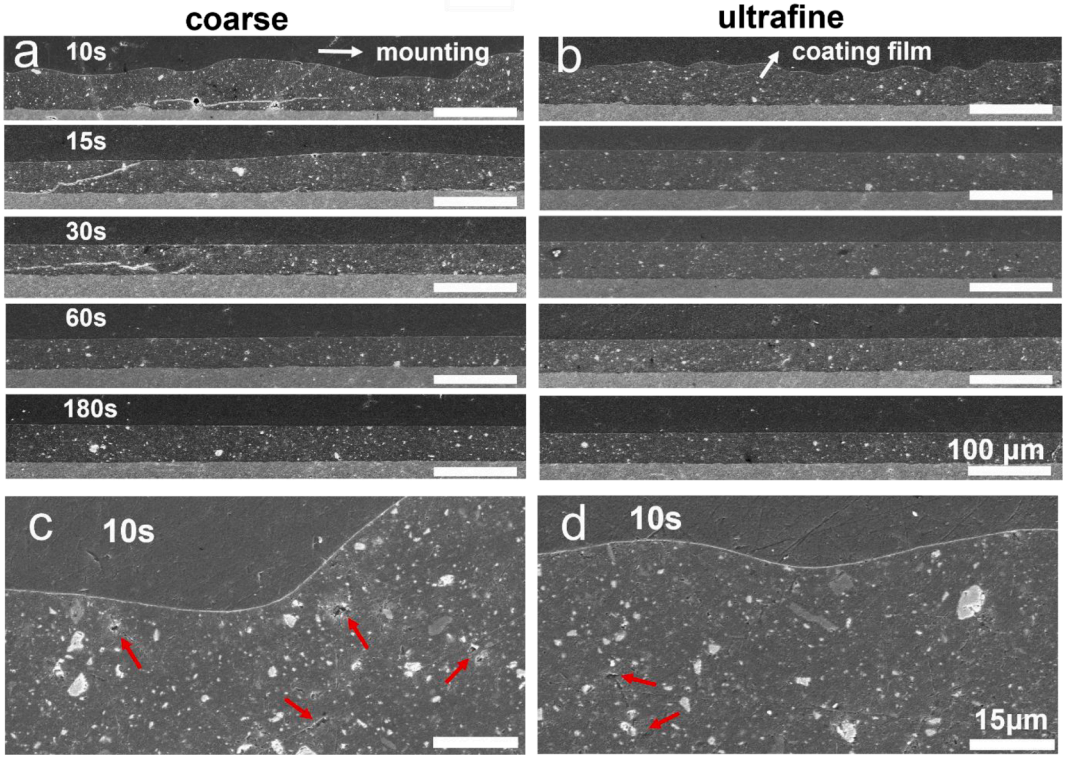

Fig. 5. SEM images of cross sections of coating films made with (a) coarse and (b) ultrafine powder at 10 s, 15 s, 30 s, 60 s and 180 s, respectively; (c) magnification of (a); (d) magnification of (b) after leveling for 10 s.

shrinkage [58]. But the relatively large air pockets cannot fully dissolve and escape during curing and therefore cause voids. As can be seen from Fig. 5a, the melting finished in the first 10 s. The trapped air mainly escaped during this stage, leaving few voids inside the coating film as shown by the red arrows in Fig. 5c. As merging and leveling continued, the top surface became flatter while the inner structure formed fewer voids. (Fig. 5c and 5d, Fig. S2). The ultrafine powder coating films demonstrate fewer surface variations after melting and fewer inner voids throughout the curing process than the coarse ones (Fig. 5b and d). Optical microscopy images of the coating films show that the coating films first became flat and then rough during successive curing (Fig. 6a and c). From 10 s to 60 s, the hills merged and became broader but lower hills, resulting in an apparent orange peel effect. After 60 s, there formed more and more microscale bits and pits, which made the surface rough. The maximum height, Sz, dramatically decreases from 50.0 μm to 5.8 μm during curing, while the average roughness, Sa, decreases from 16.00 μm to its lowest, 0.72 μm, at 180 s before rising again as shown in the inset of Fig. 7a. Meanwhile, the ultrafine powder coating film exhibits a flatter surface (Fig. 6b and d) and lower roughness (Fig. 7a) than the one prepared with the coarse powder throughout the curing. As can be noticed, the surfaces prepared with the ultrafine powder at 15 s and 30 s look similar to the one prepared with coarse powder at 30 s and 60 s, respectively. This finding indicates that the ultrafine powder coating films level and degas faster than the ones with the coarse powder. It is because the loose packing of particles and smaller average air pockets among particles induced from the smaller particle size enable the particles to be heated evenly, to coalesce quickly and to release air easily [1]. On the contrary, the larger particles have larger average air pockets among particles. Especially, the relatively large air pockets larger than 15 μm, could severely impair the coalesce of the melted particles and result in more voids inside the coating films.

Leveling of the coating films causes a change to the coating's gloss as well. As can be seen from Fig. 7b, the gloss increases dramatically at the beginning of the curing, reaches the peak at about 60 s, and then gradually decreases. The initial increase of the gloss is likely caused by leveling of the melt, and the subsequent decrease is attributed to the formation of micro bits and pits. It is very impressive that the ultrafine coating film achieves a gloss of 96.1, while the coarse one reaches 91.2 at 60 s. This is mainly because leveling of the melt almost finishes during the first 60 s, but the crosslinking reactions just start, and the decrease of gloss caused by the crosslinking and formation of micro bits and pits is still inapparent. Coatings prepared with ultrafine particles demonstrate faster leveling and therefore higher gloss than that of coatings prepared with coarse particles. Both the decrease of gloss after 60 s and the formation of micro bits and pits could occur for three reasons. The first is the local vortex, the flow direction of which is opposite to that of the melt, and therefore preventing its further leveling. The second is the ongoing degassing which removes residual air from inner structure (Fig. 5 and Fig. S2), but the melt, due to the cross-linked polymeric structure, could not fully recover its surface. The third is the uneven distribution of fillers. The integrated optical microscopy, Micro-CT and CLSM study characterized the distribution of filler and surface morphology at the same site, and as can be seen from Fig. 8, microscale variations on the coating surface are closely related to the presence of large particles under the coating. Bits usually appeared in filler-rich areas while pits are in filler-poor areas. In general, these three reasons contribute to the rougher surfaces at the later stage of curing.

3.4. Anti-corrosion performance

Salt spray is the most commonly used method in the coating industry to measure corrosion resistance. Fig. 9 illustrates the salt spray results after 500 h exposure in salt fog. It is observed that the ultrafine powder coating panels demonstrate narrower corrosion creepage. By utilizing ultrafine powder, the creepage decrease from about 1.06 mm to about 0.68 mm, an ~30 % decrease.

Electrochemical Impedance Spectroscopy (EIS) has been proven effective in estimating the corrosion protection behavior of organic coatings films [49,59–61]. Generally, a larger modulus of resistance at 0.01 Hz, and a closer to −90° phase angle at high frequency domain indicate better corrosion protection for barrier type coating films. In particular, a higher impedance at the early stage of immersion, usually after ~10 days, foretells a better long-term coating performance [49,62–64].

The Bode-modulus and Bode-phase plots are shown in Fig. 10a–d. The ultrafine powder coating panel demonstrates larger modulus of resistance at 0.01 Hz (8.0×10^{10} Ω cm^2) than the coarse one (1.4×10^{10} Ω cm^2), and boarder plateau of phase angle close to −90° at high frequency domain, which indicate that ultrafine powder coatings have better barrier effect and corrosion protection for the steel than the coarse

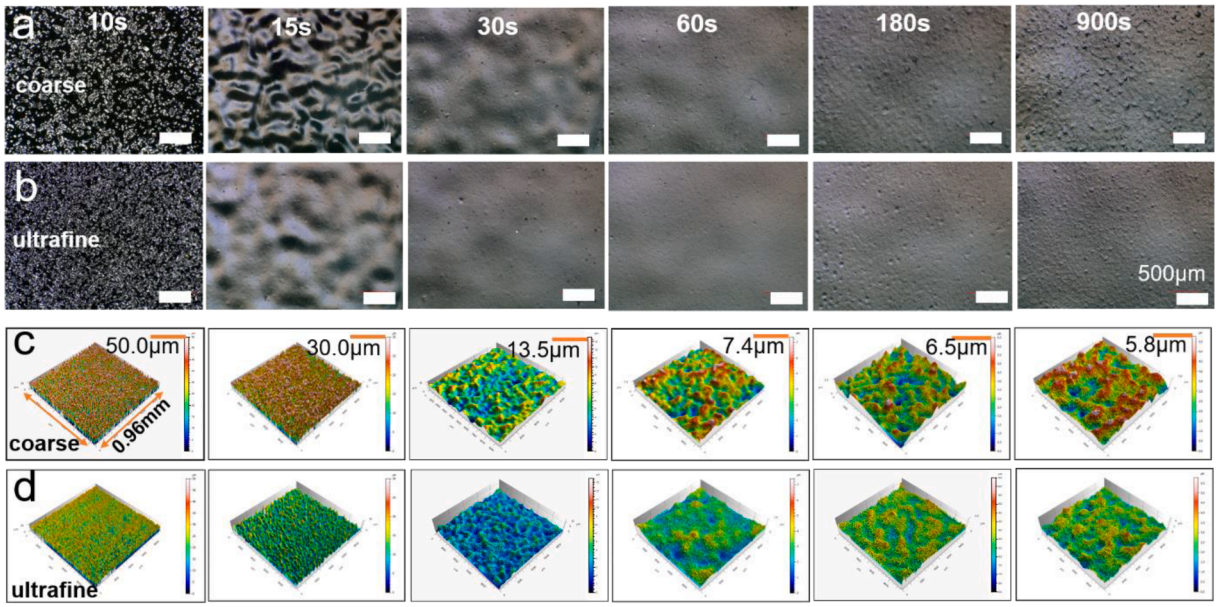

Fig. 6. Optical images of the (a) coarse and (b) ultrafine powder cured for different time. 3D CLSM images of the coating films made with (c) coarse and (d) ultrafine powder cured for different time.

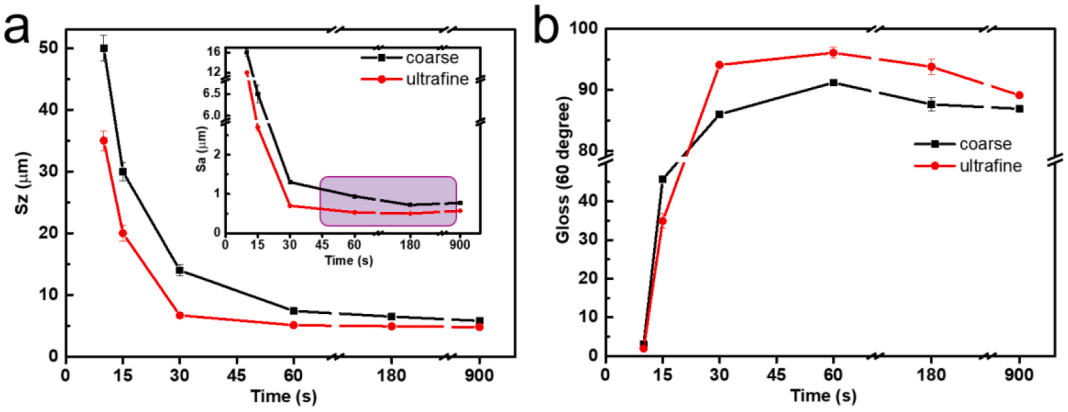

Fig. 7. (a) Sz and Sa and (b) gloss of the coarse and ultrafine powder coating films during curing.

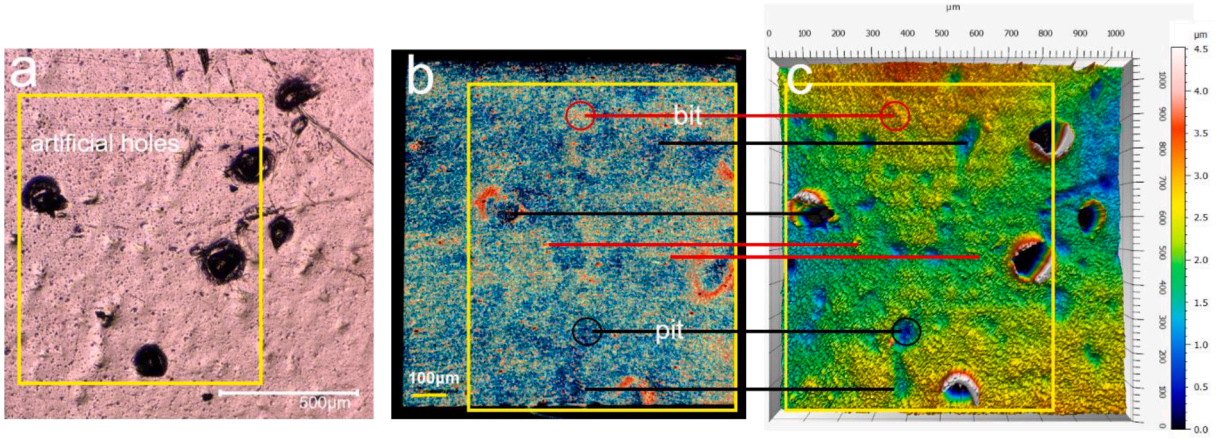

Fig. 8. (a) Optical (b) micro-CT and (c) CLSM images of the PE high gloss coarse coating with artificial holes for positioning.

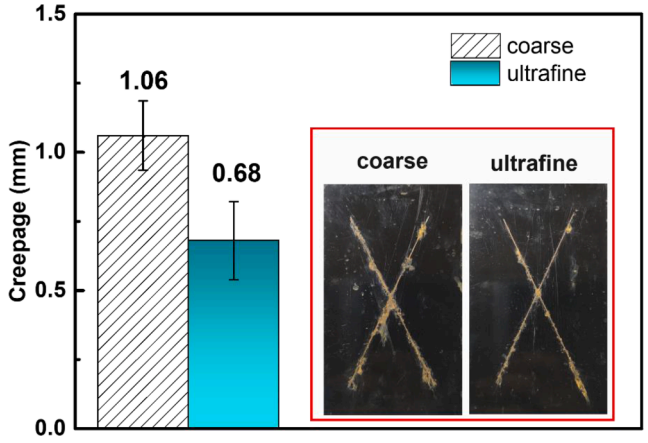

Fig. 9. Creepage of the ultrafine and coarse powder coating panels after salt spray tests for 500 h. The insets are optical images for coarse and ultrafine coating panels after salt spray tests.

one [65].

The obtained fitting results for R_{pore} and R_{ct} are shown in Fig. 10e and f. At the beginning of immersion, the R_{pore} for the ultrafine (1.1×10^{11} Ω cm^2) is about one order of magnitude larger than that for the coarse (1.5×10^{10} Ω cm^2). Even after 54 days of immersion, the R_{pore} for the ultrafine is still about one order of magnitude larger than that for the coarse. This larger R_{pore} indicates that the amount of corrosive species such as Cl^-, H_2O and O_2 penetrated the coatings is significantly decreased, indicating better barrier effects provided by the ultrafine powder coatings. In addition, the value of R_{ct} for the ultrafine powder coating is about half to one order of magnitude larger than that for the coarse throughout the immersion period. R_{ct} is normally inversely proportional to the corrosion rate of the specimen. This higher R_{ct} value means that the charge transfer reaction is sluggish, inferring the denser ultrafine powder coating film can retard the penetration of corrosion species, and therefore improving the anticorrosion performance [66].

The narrower creepage during salt spray tests and higher barrier effects in electrochemical tests confirm that the ultrafine powder coating films have better corrosion resistance than do the coarse ones. The mechanisms for the enhanced corrosion performance are shown in Fig. 11. One reason is that the ultrafine particles demonstrate looser packing (Fig. 5d) with smaller average air pockets (Fig. 5f) during spray (Fig. 11a and b) and faster degassing and leveling during curing (Fig. 6b). These two aspects offer denser structure for the obtained coating films (Fig. 3b, Fig. 11c and d). As a result, the enhanced barrier effect (Fig. 10) prevents the rapid ingress of electrolytes (Fig. 11e and f). The other is that the ultrafine particles have more uniform deposition (Fig. 5b) and faster leveling during curing, which induce lower surface roughness (Fig. 2b and g, Fig. 11d), and therefore result in higher effective dry film thickness of ultrafine powder coating films with the same measured film thickness. These two aspects of reasons contribute to the smooth surface, dense structure, and enhanced corrosion resistance of the ultrafine powder coatings.

4. Conclusions

This is the first report to investigate the formation mechanisms of

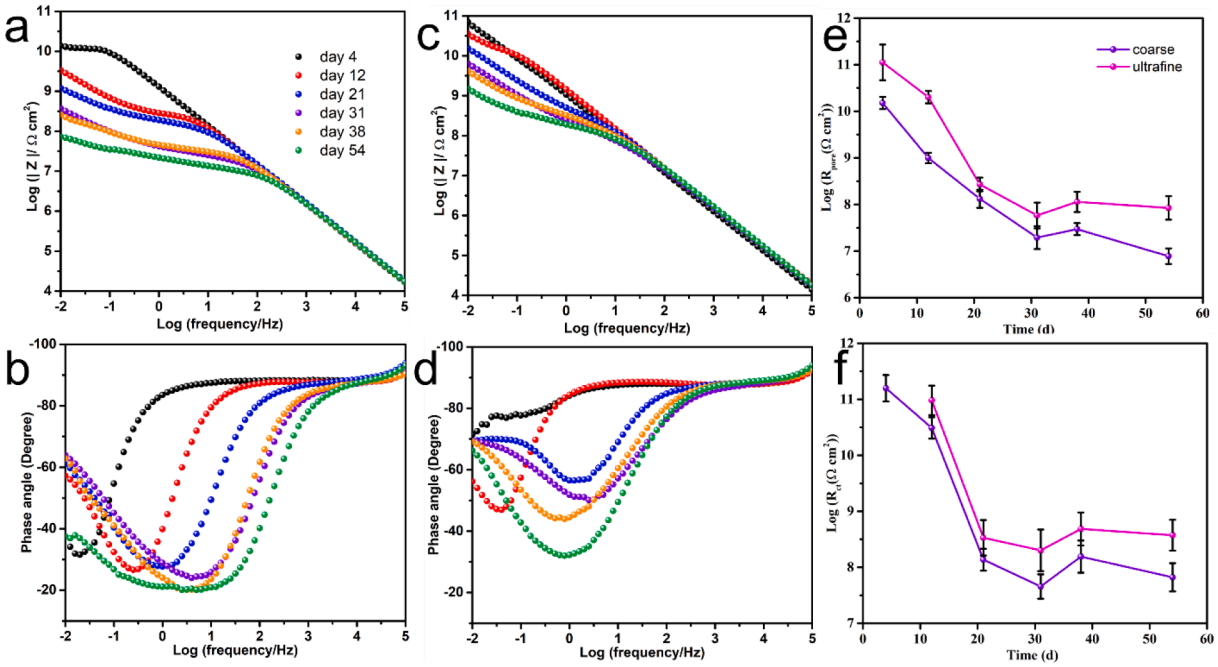

Fig. 10. (a) Bode-modulus plots and (b) Bode-phase plots of high gloss coarse coatings. (c) Bode-modulus plots and (d) Bode-phase plots of high gloss ultrafine coatings. (e) R_{pore} and (f) R_{ct} of high gloss coarse and ultrafine coatings versus immersion time in 3.5% NaCl solution.

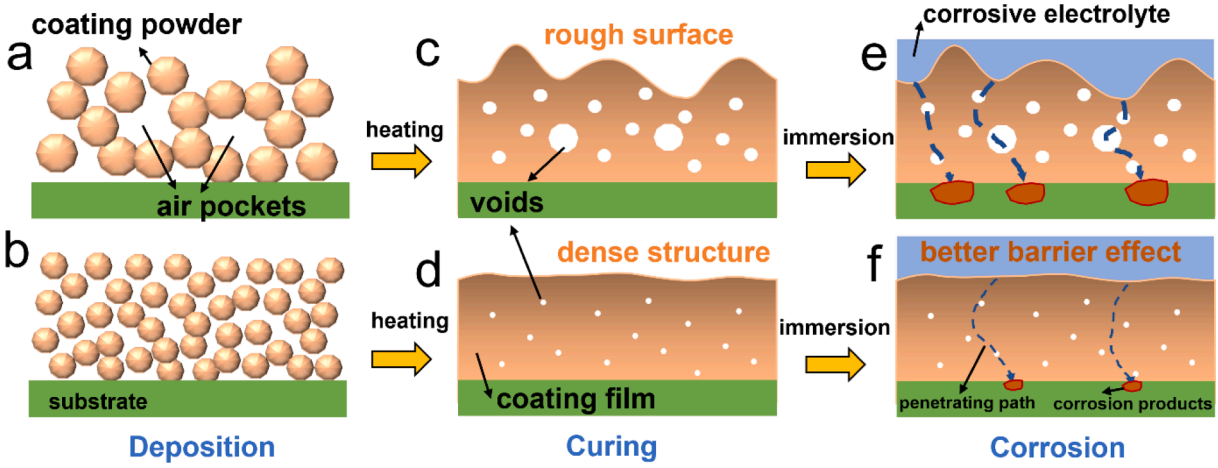

Fig. 11. The proposed mechanisms for particle deposition (a, b), curing (c, d) and corrosion (e, f) for the coarse (a, c and e) and ultrafine powder coatings (b, d and f).

smoother surfaces created by ultrafine powders in terms of deposition during spray and leveling during curing, and to analyze the impacts of ultrafine powders on film structures and corrosion performance. The ultrafine powder, due to the smaller particle size and larger charge to mass ratio, demonstrates looser and more uniform packing with smaller average air pockets during spray, and accelerated leveling and degassing during curing when compared to the coarse powder. This deposition and leveling behavior results in a lower surface roughness, higher gloss, denser structure, and higher corrosion resistance, i.e., higher barrier properties and narrower salt spray creepage. Coatings that utilizing ultrafine powders show remarkable improvements over their coarse counterparts in terms of surface qualities and corrosion performances. The improved coating properties would benefit coating manufacturers by producing thin film finishing with enhanced decoration and protection and would expend the applications of powder coatings in many industries such as electronics and automotive industries.

Declaration of Competing Interest

The authors declare that they have no known competing financial interests or personal relationships that could have appeared to influence the work reported in this paper.

Data availability

Data will be made available on request.

Acknowledgements

The authors thank for the funding from China Scholarship Council (CSC) (No. 201707040063), The Natural Sciences and Engineering Research Council of Canada (Grant No. RGPIN-2018-06256 and RGPIN-2018-06672), and Zhengzhou University, China, as well as technical supports from Chemistry Department and Surface Science Western at the University of Western Ontario.

Appendix A. Supplementary data

Supplementary data to this article can be found online at https://doi.org/10.1016/j.cej.2022.140815.

References

[1] E. Spyrou. Powder Coatings Chemistry and Technology. 3rd ed. Vincentz Network. 2012. https://doi.org/10.1515/9783748602361.

[2] C.K. Schoff, Organic coatings: The paradoxical materials, in: Progress in Organic Coatings, Elsevier, 2005, pp. 21–27, https://doi.org/10.1016/j.porgcoat.2004.05.001.

[3] T.A. Misev, R. Van Der Linde, Powder coatings technology: New developments at the turn of the century, Prog. Org. Coat. 34 (1997) 160–168, https://doi.org/10.1016/S0300-9440(98)00029-0.

[4] J. Fu, M. Krantz, H. Zhang, J. Zhu, H. Kuo, Y.M. Wang, K. Lis, Investigation of the recyclability of powder coatings, Powder Technol. 211 (2011) 38–45, https://doi.org/10.1016/j.powtec.2011.03.016.

[5] G. Crapper, Powder Coatings, in: Polymer Science: A Comprehensive Reference, 10 Volume Set, Elsevier, 2012: pp. 541–566. https://doi.org/10.1016/B978-0-444-53349-4.00279-X.

[6] H. Marchebois, S. Joiret, C. Savall, J. Bernard, S. Touzain, Characterization of zinc-rich powder coatings by EIS and Raman spectroscopy, Surf. Coat. Technol. 157 (2002) 151–161, https://doi.org/10.1016/S0257-8972(02)00147-0.

[7] P.T. ELLIOTT, J.E. GLASS, WATER-BORN COATINGS, Applied Polymer Science: 21st Century. (2000) 563–588. https://doi.org/10.1016/B978-008043417-9/50032-5.

[8] R. Lambourne, T.A. Strivens, Paint and surface coatings: theory and practice, Elsevier, 1999.

[9] P.A. Sørensen, S. Kiil, K. Dam-Johansen, C.E. Weinell, Anticorrosive coatings: A review, J. Coat. Technol. Res. 6 (2009) 135–176, https://doi.org/10.1007/s11998-008-9144-2.

[10] H. Zhang, M.S. Yang, M.T.I. Bhuiyan, J. Zhu, CHAPTER 15: Green Chemistry for Automotive Coatings: Sustainable Applications, RSC Green Chemistry, 2019, pp. 368–394.

[11] J. Zhu, H. Zhang, Ultrafine powder coatings: an innovation, Powder, Coating. 16 (2005) 39–47.

[12] H.C. Hamaker, The London-van der Waals attraction between spherical particles, Physica 4 (1937) 1058–1072, https://doi.org/10.1016/S0031-8914(37)80203-7.

[13] J. Visser, Van der Waals and other cohesive forces affecting powder fluidization, Powder Technol. 58 (1989) 1–10, https://doi.org/10.1016/0032-5910(89)80001-4.

[14] J. Zhu, Fluidization of fine powders, in: Granular Materials, Royal Society of Chemistry, 2007, pp. 270–295, https://doi.org/10.1039/9781847550996-00270.

[15] D. Geldart, N. Harnby, A.C. Wong, Fluidization of cohesive powders, Powder Technol. 37 (1984) 25–37, https://doi.org/10.1016/0032-5910(84)80003-0.

[16] H. Liu, Y. Li, Q. Guo, Fluidization Quality Improvement for Cohesive Particles by Fine Powder, Coating (2006), https://doi.org/10.1021/ie050083y.

[17] Q. Huang, H. Zhang, J. Zhu, Flow properties of fine powders in powder coating, Particuology. 8 (2010) 19–27, https://doi.org/10.1016/j.partic.2009.05.007.

[18] J. Xie, H. Zhang, Y. Shao, D. Bao, H. Zhang, J. Zhu, Investigation of the performance of fumed silica as flow additive in polyester powder coatings, Coatings 10 (2020) 1–17, https://doi.org/10.3390/coatings10100977.

[19] Y. Wc, Fluidization of fine cohesive powders and nanoparticles - A review, accessed July 2, 2021, J. Chin. Inst. Chem. Eng. 36 (2005) 1–15, https://www.cheric.org/research/tech/periodicals/view.php?seq=1018730.

[20] D.K. Balachandran, L.J. Jallo, R.N. Davé, S.P. Beaudoin, Adhesion of dry nano-coated microparticles to stainless steel: A physical interpretation, Powder Technol. 226 (2012) 1–9, https://doi.org/10.1016/J.POWTEC.2012.02.035.

[21] W. Li, D.C. Franco, M.S. Yang, X. Zhu, H. Zhang, Y. Shao, H. Zhang, J. Zhu, Comparative Study of the Performances of Al(OH)3 and BaSO4 in Ultrafine Powder Coatings, Processes 2019, Vol. 7, Page 316. 7 (2019) 316. https://doi.org/10.3390/PR7050316.

[22] W. Li, Y. Shao, J. Zhu, H. Zhang, H. Zhang, Reducing comminution over-grinding of powder coatings with modified grinding pins in an air classifier mill, Powder Technol. 344 (2019) 36–45, https://doi.org/10.1016/J.POWTEC.2018.11.076.

[23] Q. Huang, A. Mesbah-Nejad, S.M. Tadayyon, P. Norton, H. Zhang, J. Zhu, Measurement of inter-particle forces by an interfacial force microscope, Particuology. 8 (2010) 400–406, https://doi.org/10.1016/j.partic.2010.05.011.

[24] Q. Huang, H. Zhang, J. Zhu, Onset of an innovative gasless fluidized bed-comparative study on the fluidization of fine powders in a rotating drum and a traditional fluidized bed, Chemical Engineering Science. 65 (2010) 1261–1273, https://doi.org/10.1016/j.ces.2009.09.083.

[25] Q. Huang, H. Zhang, J. Zhu, Experimental study on fluidization of fine powders in rotating drums with various wall friction and baffled rotating drums, Chem. Eng. Sci. 64 (2009) 2234–2244, https://doi.org/10.1016/j.ces.2009.01.047.

[26] C.C. Xu, H. Zhang, J. Zhu, Improving flowability of cohesive particles by partial coating on the surfaces, Can. J. Chem. Eng. 87 (2009) 403–414, https://doi.org/10.1002/cjce.20179.

[27] H. Duan, X. Liang, T. Zhou, J. Wang, W. Tang, Fluidization of mixed SiO2 and ZnO nanoparticles by adding coarse particles, Powder Technol. 267 (2014) 315–321, https://doi.org/10.1016/J.POWTEC.2014.07.045.

[28] Q. Yu, R.N. Dave, C. Zhu, J.A. Quevedo, R. Pfeffer, Enhanced fluidization of nanoparticles in an oscillating magnetic field, AIChE J 51 (2005) 1971–1979, https://doi.org/10.1002/AIC.10479.

[29] A. Ajbar, K. Alhumazi, M. Asif, Improvement of the Fluidizability of Cohesive Powders through Mixing with Small Proportions of Group A Particles, The, Can. J. Chem. Eng. 83 (2005) 930–943, https://doi.org/10.1002/CJCE.5450830602.

[30] X. Meng, H. Zhang, J. Zhu, The characteristics of particle charging and deposition during powder coating processes with coarse powder, J. Phys. D Appl. Phys. 41 (2008), 195207, https://doi.org/10.1088/0022-3727/41/19/195207.

[31] X. Meng, H. Zhang, J. (Jesse) Zhu, Characterization of particle size evolution of the deposited layer during electrostatic powder coating processes, Powder Technol. 195 (2009) 264–270, https://doi.org/10.1016/j.powtec.2009.06.010.

[32] X. Meng, J. (Jesse) Zhu, H. Zhang, Influences of different powders on the characteristics of particle charging and deposition in powder coating processes, J. Electrostat. 67 (2009) 663–671, https://doi.org/10.1016/j.elstat.2009.01.044.

[33] X. Meng, J. Zhu, H. Zhang, The characteristics of current density distribution during corona charging processes of different particulates, J. Phys. D Appl. Phys. 41 (2008), 172007, https://doi.org/10.1088/0022-3727/41/17/172007.

[34] X. Meng, J. Zhu, H. Zhang, The characteristics of particle charging and deposition during powder coating processes with ultrafine powder, J. Phys. D Appl. Phys. 42 (2009), 065201, https://doi.org/10.1088/0022-3727/42/6/065201.

[35] Z. Li, C. Zhang, J. Zhu, Numerical study of the effect of particle size on the coating efficiency and uniformity of an electrostatic powder coating process, Can. J. Chem. Eng. 83 (2005) 882–888, https://doi.org/10.1002/cjce.5450830510.

[36] M.S. Mozumder, H. Zhang, J. Zhu, Mimicking Lotus Leaf: Development of Micro-Nanostructured Biomimetic Superhydrophobic Polymeric Surfaces by Ultrafine Powder Coating Technology, Macromol. Mater. Eng. 296 (2011) 929–936, https://doi.org/10.1002/mame.201100080.

[37] J. Huang, M. Yang, H. Zhang, J. Zhu, Solvent-Free Fabrication of Robust Superhydrophobic Powder Coatings, ACS Appl. Mater. Interfaces 13 (2021) 1323–1332, https://doi.org/10.1021/acsami.0c16582.

[38] T. Haile, G. Nakhla, J. Zhu, H. Zhang, J. Shugg, Mechanistic study of the bactericidal action of silver-loaded chabasite on Acidithiobacillus thiooxidans, Microporous Mesoporous Mater. 127 (2010) 32–40, https://doi.org/10.1016/j.micromeso.2009.06.030.

[39] R. Yeasmin, H. Zhang, J. Zhu, H. Kazemian, Pre-treatment and conditioning of chabazites followed by functionalization for making suitable additives used in antimicrobial ultra-fine powder coated surfaces, RSC Adv. 6 (2016) 88340–88349, https://doi.org/10.1039/c6ra14295h.

[40] J. Cui, R. Yeasmin, Y. Shao, H. Zhang, H. Zhang, J. Zhu, Fabrication of Ag+, Cu2+, and Zn2+ Ternary Ion-Exchanged Zeolite as an Antimicrobial Agent in Powder Coating, Ind. Eng. Chem. Res. 59 (2020) 751–762, https://doi.org/10.1021/acs.iecr.9b05338.

[41] J. Cui, Y. Shao, H. Zhang, H. Zhang, J. Zhu, Development of a novel silver ions-nanosilver complementary composite as antimicrobial additive for powder coating, Chemical Engineering Journal. 420 (2021), 127633, https://doi.org/10.1016/j.cej.2020.127633.

[42] W. Shi, M.S. Mozumder, H. Zhang, J. Zhu, H. Perinpanayagam, MTA-enriched nanocomposite TiO2-polymeric powder coatings support human mesenchymal cell attachment and growth, Biomedical Materials (Bristol). 7 (2012), 055006, https://doi.org/10.1088/1748-6041/7/5/055006.

[43] N.Y. Hou, J. Zhu, H. Zhang, H. Perinpanayagam, Ultrafine calcium-titania-polyester dry powder coatings promote human mesenchymal cell attachment and biomineralization, Surf. Coat. Technol. 251 (2014) 177–185, https://doi.org/10.1016/j.surfcoat.2014.04.022.

[44] N.Y. Hou, J. Zhu, H. Zhang, H. Perinpanayagam, Epoxy resin-based ultrafine dry powder coatings for implants, J. Appl. Polym. Sci. 133 (2016), https://doi.org/10.1002/app.43960.

[45] Y. Luo, J. Zhu, Y. Ma, H. Zhang, Dry coating, a novel coating technology for solid pharmaceutical dosage forms, International Journal of Pharmaceutics. 358 (2008) 16–22, https://doi.org/10.1016/j.ijpharm.2008.03.028.

[46] M. Musiani, M.E. Orazem, N. Pébère, B. Tribollet, V. Vivier, Determination of resistivity profiles in anti-corrosion coatings from constant-phase-element parameters, Prog. Org. Coat. 77 (2014) 2076–2083, https://doi.org/10.1016/j.porgcoat.2013.12.013.

[47] S.G. Croll, Electrolyte transport in polymer barrier coatings: perspectives from other disciplines, Prog. Org. Coat. 124 (2018) 41–48, https://doi.org/10.1016/j.porgcoat.2018.07.027.

[48] G.W. Walter, A critical review of the protection of metals by paints, Corros. Sci. 26 (1986) 27–38, https://doi.org/10.1016/0010-938X(86)90120-4.

[49] J.R. Scully, Electrochemical Impedance of Organic-Coated Steel: Correlation of Impedance Parameters with Long-Term Coating Deterioration, J. Electrochem. Soc. 136 (1989) 979–990, https://doi.org/10.1149/1.2096897.

[50] N. Wang, D. Xiong, Y. Deng, Y. Shi, K. Wang, Mechanically robust superhydrophobic steel surface with anti-icing, UV-durability, and corrosion resistance properties, ACS Appl. Mater. Interfaces 7 (2015) 6260–6272, https://doi.org/10.1021/acsami.5b00558.

[51] X. Meng, H. Zhang, J. Zhu, J. Zhu, The characteristics of particle charging and deposition during powder coating processes with ultrafine powder, Journal of Physics D: Applied Physics To. 42 (2009) 65201, https://doi.org/10.1088/0022-3727/42/6/065201.

[52] J.F. Hughes, Electrostatic Powder Coating. 1984. https://apps.dtic.mil/sti/citations/ADA302382 (accessed July 2, 2021).

[53] B.C. Sampuran-Singh, A.W. O'Neill, Bright, A parametric study of electrostatic powder coating, J. Electrostat. 4 (1978) 325–334, https://doi.org/10.1016/0304-3886(78)90044-X.

[54] A.G. Bailey, The science and technology of electrostatic powder spraying, transport and coating, J. Electrostat. 45 (1998) 85–120, https://doi.org/10.1016/S0304-3886(98)00049-7.
[55] S. Wu, Electrostatic charging and deposition of powder coatings, Polym.-Plast. Technol. Eng. 7 (1976) 119–220, https://doi.org/10.1080/03602557608063114.
[56] R.P. Corbett, B. Makin, ELECTROSTATIC APPLICATION OF VITREOUS ENAMEL IN DRY POWDER FORM, Trans. Inst. Met. Finish. 51 (1973) 160–164, https://doi.org/10.1080/00202967.1973.11870283.
[57] M. Pauthenier, M. Moreau-Hanot, La charge des particules sphériques dans un champ ionisé, J. Phys. Radium. (1932) 590–613, https://doi.org/10.1051/jphysrad:01932003012059000ï.
[58] S. Jahromi, B. Mostert, A. Derks, F. Koldijk, Mechanism of action of benzoin as a degassing agent in powder coatings, Prog. Org. Coat. 48 (2003) 183–193, https://doi.org/10.1016/S0300-9440(03)00096-1.
[59] H.P. Hack, Defect Area Determination of Organic Coated Steels in Seawater Using the Breakpoint Frequency Method, J. Electrochem. Soc. 138 (1991) 33, https://doi.org/10.1149/1.2085574.
[60] J.M. McIntyre, H.Q. Pham, Electrochemical impedance spectroscopy; a tool for organic coatings optimizations, Prog. Org. Coat. 27 (1996) 201–207, https://doi.org/10.1016/0300-9440(95)00532-3.
[61] Y. Bao, Y. Yan, Y. Chen, J. Ma, W. Zhang, C. Liu, Facile fabrication of BTA@ZnO microcapsules and their corrosion protective application in waterborne polyacrylate coatings, Prog. Org. Coat. 136 (2019), 105233, https://doi.org/10.1016/J.PORGCOAT.2019.105233.
[62] Y. Ye, D. Zhang, Z. Liu, W. Liu, H. Zhao, L. Wang, X. Li, Anti-corrosion properties of oligoaniline modified silica hybrid coatings for low-carbon steel, Synth. Met. 235 (2018) 61–70, https://doi.org/10.1016/j.synthmet.2017.11.015.
[63] J. Zhong, G.X. Zhou, P.G. He, Z.H. Yang, D.C. Jia, 3D printing strong and conductive geo-polymer nanocomposite structures modified by graphene oxide, Carbon 117 (2017) 421–426, https://doi.org/10.1016/j.carbon.2017.02.102.
[64] G. Tian, M. Zhang, Y. Zhao, J. Li, H. Wang, X. Zhang, H. Yan, High Corrosion Protection Performance of a Novel Nonfluorinated Biomimetic Superhydrophobic Zn−Fe Coating with Echinopsis multiplex-like Structure, (2019). https://doi.org/10.1021/acsami.9b15088.
[65] N. Wang, Y. Zhang, J. Chen, J. Zhang, Q. Fang, Dopamine modified metal-organic frameworks on anti-corrosion properties of waterborne epoxy coatings, Prog. Org. Coat. 109 (2017) 126–134, https://doi.org/10.1016/j.porgcoat.2017.04.024.
[66] Z. Yang, X. Liu, Y. Tian, Novel metal-organic super-hydrophobic surface fabricated by nanosecond laser irradiation in solution, Colloids Surf A Physicochem Eng Asp 587 (2020), 124343, https://doi.org/10.1016/J.COLSURFA.2019.124343.